

# Microscopic modeling of photoluminescence of strongly disordered semiconductors<sup>\*</sup>

P. Bozsoki<sup>\*</sup>, M. Kira, W. Hoyer, T. Meier, I. Varga<sup>b</sup>,  
P. Thomas, S.W. Koch

*Department of Physics and Material Sciences Center, Philipps University, Renthof  
5, D-35032 Marburg, Germany*

<sup>b</sup>*Elméleti Fizika Tanszék, Fizikai Intézet, Budapesti Műszaki és  
Gazdaságtudományi Egyetem, Budafoki út 8, H-1111 Budapest, Hungary*

---

## Abstract

A microscopic theory for the luminescence of ordered semiconductors is modified to describe photoluminescence of strongly disordered semiconductors. The approach includes both diagonal disorder and the many-body Coulomb interaction. As a case study, the light emission of a correlated plasma is investigated numerically for a one-dimensional two-band tight-binding model. The band structure of the underlying ordered system is assumed to correspond to either a direct or an indirect semiconductor. In particular, luminescence and absorption spectra are computed for various levels of disorder and sample temperature to determine thermodynamic relations, the Stokes shift, and the radiative lifetime distribution.

*Key words:* photoluminescence, theory, disordered semiconductors, Stokes shift, lifetime, thermodynamical relation

*PACS:* 78.55.-m, 42.50.-p, 71.35.-y, 78.30.Ly

---

<sup>\*</sup> The authors are thankful to R. Zimmermann and S. D. Baranovskii for valuable discussions. This work has been supported by the Optodynamic Center of the Philipps-University Marburg, and by the Deutsche Forschungsgemeinschaft (DFG) through the Quantum Optics in Semiconductors Research Group. T. M. thanks the DFG for support via a Heisenberg fellowship (ME 1916/1). I. V. thanks for financial support from the OTKA (Hungarian Research Fund) under contract Nos. T042981 and T046303. We thank the John von Neumann Institut für Computing (NIC), Forschungszentrum Jülich, Germany, for grants for extended CPU time on their supercomputer systems.

<sup>\*</sup> Corresponding author.

*Email address:* peter.bozsoki@physik.uni-marburg.de (P. Bozsoki).

## 1 Introduction

Photoluminescence experiments are widely used as a diagnostic tool to investigate the electronic structure of semiconductors and semiconductor heterostructures in particular, also in the presence of disorder. Such measurements can, e.g., provide information about the electron-hole many-body states related to the dynamics of relaxation of the optically generated excitations. In particular, temperature-dependent spectra can be used to study localization of the optical excitations [1,2,3,4,5]. Time-resolved data and radiative lifetime distributions measured by frequency-response-spectroscopy [6] give further information about the electronic states and relevant processes in disordered semiconductors.

In order to extract meaningful information from the luminescence data, a theoretical model which incorporates the relevant physical processes is required. Starting from a model which is able to reproduce the main features of the experimental data for reasonable parameters, one tries to arrive at a possible interpretation. So far, dynamical aspects as well as spectral signature of the photoluminescence of disordered semiconductors have usually been computed using Monte-Carlo approaches [1,7,8,9,10,11,12]. The underlying model is either based on excitonic excitations [1,7,8,9] or, alternatively, independent electron and hole excitations are assumed [10,11,12].

The Monte Carlo methods, discussed above, phenomenologically describe the following processes: (i) The photo-excitation with excess energy creates electron-hole pairs in states that are energetically well above the emitting states. (ii) Depending on the material system under study, fast incoherent relaxation of either excitons or independent electrons and holes into energetically lower lying states close to the band edges is assumed. (iii) As these states are presumably localized in disordered semiconductors in the absence of coupling to phonons, a slower phonon-induced relaxation among these states takes place which is governed by their mutual distance, the localization length, the energetic density of states, and the temperature. (iv) These relaxation processes compete with radiative and non-radiative recombination. In the exciton picture, the radiative recombination rate is given by the intrinsic structure, i.e., by the optical matrix elements of the correlated electron-hole pair [1]. For independent electrons and holes it is their mutual distance that determines their recombination rate via a radiative tunneling process [10].

This scenario suggests the following model parameters: localization length (sometimes allowed to depend on energy), total density of localized states in the band tails, the form of the density of states in the tail region, and an attempt-to-escape frequency determining the phonon-induced tunneling (hopping) into energetically higher or lower lying states. By choosing a model and

fitting the simulated spectra to experimental ones one finds a combination of parameters which represent the data in an optimal way. The model and its parameters can be further substantiated if one succeeds to reproduce simultaneously data for various temperatures and also time resolved spectra.

Although this procedure is widely used and has been successfully applied in many cases e.g. [1,7,8,9], it is not very satisfactory from a more fundamental point of view. Instead of using a phenomenological description, one should be able to analyze the luminescence of disordered semiconductors using a microscopic approach which is based on a more realistic model of a disordered structure. An attempt into this direction has been presented by Zimmermann and Runge [2] who have used an exciton picture for the case of a weakly disordered system. An adequate and comprehensive microscopic theory for the luminescence in the presence of disorder should simultaneously include the phonon-induced relaxation, radiative and non-radiative recombination, and the many-particle Coulomb interaction. Microscopic approaches have recently been presented on the basis of an effective-mass approach considering both bound-excitonic and separate electron-hole recombination processes. [13,14].

For the case of perfectly ordered systems, a microscopic theory of semiconductor luminescence has been developed recently [15,16,17,18]. Although microscopic aspects of the Coulomb and electron-phonon interactions have been included in this approach, it is by no means trivial to extend this theory to disordered structures since one can calculate the single-particle eigenstates only for relatively small systems. In addition, an adequate analysis of the phonon-induced relaxation in a disordered system requires the treatment of many-acoustic-phonon-induced hopping processes in a system of interacting electrons, because energy differences involved in the relaxation processes in strongly disordered semiconductors are much larger than the Debye energy. A fully microscopic theory meeting these challenges does not yet exist.

As a step towards this goal, we present in this paper a treatment of luminescence in a one-dimensional tight-binding model of a disordered two-band semiconductor. We do not intend to model any existing bulk semiconductor or semiconductor heterostructure. We rather perform a case study, which treats disorder and Coulomb interaction on an equal footing. Applying the theory worked out in [15,16,17,18,19,20] for ordered semiconductors we arrive at an expression that describes radiative electron-hole recombination in a disordered system without the necessity to separately modelling bound excitonic vs. separate-pair (plasma) processes (see, e.g., [14] for such an approach). The price we have to pay is to completely neglect the explicit description of phonon-induced relaxation and hopping processes. Instead, a stationary situation which is characterized by static populations of the states is assumed. These are modeled by quasi-equilibrium Fermi-Dirac distributions for electrons and holes, implicitly assuming that the relaxation and intraband dynamics of

carriers is much faster than the radiative process. It is known that the initial relaxation is fast, i.e., on the order of ps [14,21]. In our model, we assume that this is also the case for subsequent steps such that quasi-stationary thermal single-particle distributions are always maintained. In the present paper, we do not discuss the interesting and important issue of exciton formation. From previous publications which investigated ordered semiconductors [17,19,20], it is known that: i) exciton formation is relatively slow, particularly for temperatures above 30 K. ii) Even when an appreciable amount of excitons is present, the optically active ones recombine rapidly leaving behind a correlated plasma as the dominating source of luminescence in many experimentally-relevant situations.[18] iii) In addition, the spectral positions of the dominant emission resonances do not strongly depend on the microscopic source, i.e., are similar for excitonic and independent electron and hole populations. Thus, our luminescence analysis should be reasonable for the case of quasi-stationary situations in which optically active exciton populations can be neglected. In ordered semiconductors, such conditions are typically realized for sufficiently high sample temperatures.[18] For situations in which exciton populations dominate, our results are expected to underestimate the strength of the excitonic resonance, however, the peak position should be correctly described.

The semiconductor model is based on an ordered system that can either be chosen to represent semiconductors with a direct or an indirect band gap. We can, therefore, study to what extent, as function of the strength of the disorder, the direct or an indirect nature of the model influences the luminescence and the absorption spectra. This allows us to discuss in detail the structure of the luminescence and absorption spectra, their thermodynamic relation, the dependence on the model parameters, the Stokes shift, and the radiative lifetime distribution for emission from an electron-hole plasma.

This paper is organized as follows: The model and the theoretical approach are described in Section 2 and Section 3, respectively. The results are presented and discussed in Section 4. This work ends with a discussion in a concluding Section 5 that also presents an outlook for further work.

## 2 The model

We consider a one-dimensional tight-binding model of a disordered two-band semiconductor. The total Hamiltonian is

$$\widehat{H}_{\text{total}} = \widehat{H}_0 + \widehat{H}_{\text{Cb}} + \widehat{H}_{\text{EM}}. \quad (1)$$

Here,  $\widehat{H}_0$  is the single-particle Hamiltonian describing the valence ( $h$ ) and the conduction ( $e$ ) band,

$$\widehat{H}_0 = \sum_{\alpha} \epsilon_{\alpha}^e \widehat{e}_{\alpha}^{\dagger} \widehat{e}_{\alpha} + \sum_{\beta} \epsilon_{\beta}^h \widehat{h}_{\beta}^{\dagger} \widehat{h}_{\beta}, \quad (2)$$

where  $\widehat{e}_{\alpha}^{\dagger}$  ( $\widehat{e}_{\alpha}$ ) and  $\widehat{h}_{\beta}^{\dagger}$  ( $\widehat{h}_{\beta}$ ) denote electron and hole creation (annihilation) operators, respectively. In Eq. (1), the Coulomb interaction among carriers is described by  $\widehat{H}_{\text{Cb}}$  and  $\widehat{H}_{\text{EM}}$  represents the Hamiltonian of the electromagnetic field and its interaction with the carrier system.

The single-particle eigenstates  $|\alpha e\rangle$  and  $|\beta h\rangle$  with the respective eigenvalues  $\epsilon_{\alpha}^e$  and  $\epsilon_{\beta}^h$  are obtained by diagonalizing the tight-binding Hamiltonian in the site-representation

$$\widehat{H}_0 = \sum_i \eta_i^e \widehat{e}_i^{\dagger} \widehat{e}_i + J^e \sum_{\langle ij \rangle} \widehat{e}_i^{\dagger} \widehat{e}_j + \sum_i \eta_i^h \widehat{h}_i^{\dagger} \widehat{h}_i + J^h \sum_{\langle ij \rangle} \widehat{h}_i^{\dagger} \widehat{h}_j \quad (3)$$

which contains the energies  $\eta_i^{e,h}$  of the isolated sites contributing to the conduction and valence bands, respectively, and the nearest-neighbor couplings  $J^{e,h}$  in these bands. The system consists of  $N$  sites, and periodic boundary conditions are applied. In Eq. (3), the notation  $\langle ij \rangle$  indicates that the sums are limited to the nearest neighbors. For an ordered semiconductor structure, all  $\eta_i^e$  and all  $\eta_i^h$  are taken to be identical. For the description of disorder, the site energies are randomly varied within a prescribed range. We consider only diagonal disorder, i.e., the coupling strength  $J^{e,h}$  remains unchanged under all conditions. A pictorial view of this tight-binding model is shown in Fig. 1.

At this point a remark is on order. The sites of our tight-binding model do not represent atoms. They rather represent building blocks which allow us to model the band structure of the ordered system close to the band extrema defining the gap with reasonable effective masses by choosing the nearest-neighbor couplings  $J^{e,h}$  and their nearest-neighbor separation  $a$  appropriately (see next subsection).

In the site-representation, the many-body Coulomb interaction reads

$$\widehat{H}_{\text{Cb}} = \frac{1}{2} \sum_{i,j} \sum_{\lambda} V_{ij} \widehat{a}_{\lambda i}^{\dagger} \widehat{a}_{\lambda j}^{\dagger} \widehat{a}_{\lambda j} \widehat{a}_{\lambda i} - \sum_{i,j} V_{ij} \widehat{e}_i^{\dagger} \widehat{h}_j^{\dagger} \widehat{h}_j \widehat{e}_i, \quad (4)$$

where only monopole-monopole terms have been included. In Eq. (4), the first sum with  $\lambda = e, h$  and  $\widehat{a}_{ei}^{\dagger} = \widehat{e}_i^{\dagger}$ ,  $\widehat{a}_{eh}^{\dagger} = \widehat{h}_i^{\dagger}$ , etc., represents the repulsive Coulomb interaction for carriers within one band and the second term describes the attractive Coulomb interaction between electrons and holes. The

regularized Coulomb matrix element considered here is given by

$$V_{ij} = \frac{U_0}{|i-j|a + a_0}, \quad (5)$$

with a positive constant  $U_0$ . Here,  $a$  is the nearest-neighbor site-separation and the term  $a_0 = 0.5a$  removes the unphysical singularity of the lowest excitonic bound state arising from the restriction to monopole-monopole terms in one dimension. In a one-dimensional semiconductor quantum wire it takes into account the finite cross section of the structure [22].

In the single-particle eigenbasis, the interaction Hamiltonian reads for our two-band model

$$\widehat{H}_{\text{Cb}} = \frac{1}{2} \sum_{\alpha, \beta} \sum_{\alpha', \beta'} \left[ \sum_{\lambda} V_{\alpha, \beta}^{\alpha', \beta'}(\lambda, \lambda) \widehat{a}_{\lambda\alpha}^\dagger \widehat{a}_{\lambda\beta'}^\dagger \widehat{a}_{\lambda\beta} \widehat{a}_{\lambda\alpha} - 2V_{\alpha, \beta}^{\alpha', \beta'}(e, h) \widehat{e}_{\alpha'}^\dagger \widehat{h}_{\beta'}^\dagger \widehat{h}_{\beta} \widehat{e}_{\alpha} \right], \quad (6)$$

where

$$V_{\alpha, \beta}^{\alpha', \beta'}(\lambda, \lambda') = \sum_{i, j} \psi_{\alpha'}^{\lambda*}(i) \psi_{\beta'}^{\lambda'*}(j) V_{ij} \psi_{\beta}^{\lambda'}(j) \psi_{\alpha}^{\lambda}(i) \quad (7)$$

and the  $\psi_{\alpha}^{\lambda}(i) = \langle i | \alpha \lambda \rangle$  are the single-particle eigenstates of  $\widehat{H}_0$  in site representation. As we are interested in the low-density regime, the repulsive part of the interaction is omitted in the remainder of this paper.

For the calculation of optical absorption and luminescence spectra, we also need the Hamiltonian contributions related to the quantized light field and the light-matter interaction. They are given by

$$\widehat{H}_{\text{EM}} = \widehat{H}_{\text{F}} + \widehat{H}_{\text{D}} \quad (8)$$

with the free field Hamiltonian

$$\widehat{H}_{\text{F}} = \sum_q \hbar \omega_q \left( \widehat{b}_q^\dagger \widehat{b}_q + \frac{1}{2} \right) \quad (9)$$

and the light-matter interaction in dipole approximation,

$$\widehat{H}_{\text{D}} = - \sum_{\alpha, \beta} \sum_q i \mathcal{E}_q \mu_{\alpha\beta} \widehat{e}_{\alpha}^\dagger \widehat{h}_{\beta}^\dagger \widehat{b}_q + \sum_{\alpha, \beta} \sum_q i \mathcal{E}_q \mu_{\alpha\beta}^* \widehat{h}_{\beta} \widehat{e}_{\alpha} \widehat{b}_q^\dagger. \quad (10)$$

Here, the photon creation and annihilation operators are denoted by  $\widehat{b}_q^\dagger$  and  $\widehat{b}_q$ , respectively,  $\mathcal{E}_q = \sqrt{\hbar \omega_q / 2 \epsilon_0}$  is the vacuum-field amplitude [16] and  $\mu_{\alpha\beta}$

denotes the optical matrix element between single-particle eigenstates. The latter is obtained by transforming the optical matrix elements in site representation,  $\mu_{ij}$ , into the the basis of the single-particle eigenstates. We take  $\mu_{ij} = \mu_0\delta_{ij}$  for simplicity. Note that within this approach it is not necessary to consider radiative excitonic vs. plasma recombination separately. Both processes are equally well contained in the total Hamiltonian. For details see [15,16,17,18,19,20].

### 2.1 The underlying ordered system

The ordered system is described by  $\eta_i^e = \eta_0/2$  and  $\eta_i^h = \eta_0/2$ . By choosing the sign of the coupling matrix element according to either  $\text{sgn}(J^e) = \text{sgn}(J^h)$  or  $\text{sgn}(J^e) = -\text{sgn}(J^h)$ , one can describe a direct or indirect semiconductor, respectively; see Figs. 2 and 3. Note that we are applying the electron-hole picture. The parameters are chosen such that realistic effective masses are obtained while a numerical treatment remains feasible. The system has a length  $L = Na$  and periodic boundary conditions are applied. In a tight-binding model the effective mass is given by

$$m_{\text{eff}}^\lambda = \frac{\hbar^2 N^2}{2|J^\lambda|L^2} = \frac{\hbar^2}{2|J^\lambda|a^2}. \quad (11)$$

Since each site supports a single state in the valence band and a single state in the conduction band, the number of eigenstates and thus the number of optical transitions is determined by  $N$ . The numerical computations are limited to a maximum number of sites  $N_{\text{max}}$ . Therefore, our calculated spectra correspond to a series of discrete transitions in the ordered system instead of a true continuum. The combination  $|J^\lambda|L^2/N^2$  determines the effective masses in the band  $\lambda$ . Calculations are only meaningful if their results do not critically depend on  $N$  for fixed  $|J^\lambda|L^2/N^2$ . This condition is fulfilled for all choices of the parameters used in this paper:  $N = 10$  to  $N = 30$ ,  $a = 5$  nm,  $|J^e| = 8$  meV,  $|J^h| = 8/3$  meV, leading to effective masses

$$\frac{m_{\text{eff}}^e}{m_e} = 0.17, \quad \frac{m_{\text{eff}}^h}{m_e} = 0.51, \quad (12)$$

where  $m_e$  is the free electron mass. In a realistic semiconductor, the masses determine the (three-dimensional) exciton binding energy

$$E_B = \frac{e^4 m_r}{2\epsilon_{\text{bg}} \hbar^2} \quad (13)$$

with the background permittivity  $\epsilon_{\text{bg}}$  and the reduced mass given by

$$\frac{1}{m_r} = \frac{1}{m_{\text{eff}}^e} + \frac{1}{m_{\text{eff}}^h}. \quad (14)$$

In our model the numerical value of the binding energy is adjusted to be close to  $E_B \simeq 10$  meV by choosing an appropriate factor  $U_0$  in  $V_{ij}$ .

Again we would like to point out that the values chosen for the effective masses and the exciton binding energy characterizing the many-particle interaction do not refer to any specific semiconductor structure but rather serve as pure model parameters in this case study.

## 2.2 The disordered system

The disordered system is modeled by assigning random values drawn from a box distribution of width  $W^e$  and  $W^h$  to the site energies  $\eta_i^e$  and  $\eta_i^h$ , respectively[23]. In the present paper, only uncorrelated disorder is modeled by choosing electron and hole energies independently of one another. In principle, however, also correlated or anticorrelated disorder could be used, where the upper and lower energies of one site deviate in opposite or equal directions from their average values on an absolute energy scale.

We scale the disorder energies with the reciprocal masses according to

$$\frac{W^e}{W^h} = \frac{|J^e|}{|J^h|} \quad (15)$$

in order to model disorder due to fluctuations of confinement in quantum-confined heterostructures. The dimensionless parameter

$$\frac{W}{J} = \frac{W^\lambda}{J^\lambda} \quad (16)$$

characterizes the strength of the disorder. In the following, we use the term of a “direct-based model” (“indirect-based model”) if the underlying ordered semiconductor is a direct (indirect) one, i.e., depending on whether  $J^e$  and  $J^h$  have equal or opposite sign.

In some figures, we show configurationally averaged data in order to smooth out the mesoscopic fluctuations due to small system size. This is achieved by drawing  $M$  different realizations of disorder energies from a given distribution and averaging over the calculated spectra. We also study the full distribution of certain features instead of averages.



### 3 Microscopic theory for absorption and photoluminescence

#### 3.1 Absorption

The linear optical absorption can be calculated in a semiclassical framework from the optical polarization

$$P = \langle \hat{P} \rangle = \sum_{\alpha\beta} (\mu_{\alpha\beta}^* P_{\alpha\beta} + \mu_{\alpha\beta} P_{\alpha\beta}^*), \quad (17)$$

with

$$P_{\alpha\beta} = \langle \hat{p}_{\alpha\beta} \rangle = \langle \hat{h}_\beta \hat{e}_\alpha \rangle. \quad (18)$$

The interband coherence  $P_{\alpha\beta}$  is obtained by solving the semiconductor Bloch equation [21]

$$i\hbar \frac{\partial}{\partial t} P_{\alpha\beta} = (\epsilon_\alpha^e + \epsilon_\beta^h - i\gamma) P_{\alpha\beta} - \sum_{\alpha'\beta'} V_{\alpha'\beta'}^{\alpha\beta} P_{\alpha'\beta'} - \mu_{\alpha\beta} E(t), \quad (19)$$

written in the single-particle eigenbasis, where  $\gamma = \hbar/\tau$  is a phenomenological dephasing term. Here, we have used the low-intensity limit, i.e.,  $P$  is linear in the field  $E(t)$ , and thus neglected all intraband densities of the form  $\langle a_{\lambda,\alpha}^\dagger a_{\lambda,\alpha'} \rangle$ . Furthermore, we have not included microscopic Coulomb scattering, but used the constant damping instead.

Equation (19) can be solved analytically via Fourier transformation. The solution is obtained most easily by introducing the exciton pair basis  $\Phi^\nu$  given by the solution of the source-free (homogeneous) part of Eq. (19)

$$\sum_{\alpha',\beta'} M_{\alpha\beta}^{\alpha'\beta'} \Phi_{\alpha'\beta'}^\nu = \epsilon_\nu \Phi_{\alpha\beta}^\nu, \quad (20)$$

with

$$M_{\alpha\beta}^{\alpha'\beta'} = \delta_{\alpha\alpha'} \delta_{\beta\beta'} (\epsilon_\alpha^e + \epsilon_\beta^h) - V_{\alpha'\beta'}^{\alpha\beta}. \quad (21)$$

Note, that we do not apply a factorization into relative and center-of-mass wave functions. Instead,  $\Phi^\nu$  and  $\epsilon_\nu$  denote the  $\nu^{\text{th}}$  two-particle eigenstate and eigenenergy, respectively, i.e.,

$$\Phi_{\alpha\beta}^\nu = (\langle \alpha e | \otimes \langle \beta h |) | \Phi^\nu \rangle \quad (22)$$

is the two-particle eigenstate projected onto the single-particle pair-state basis in the Hilbert space  $\mathcal{H}^e \otimes \mathcal{H}^h$ .

Using Eq. (20), we can analytically invert the Fourier transform of Eq. (19) and obtain

$$\chi''(\omega) = \sum_{\nu} \frac{|\mu_{\nu}|^2}{\epsilon_{\text{bg}}} \frac{\gamma}{(\epsilon_{\nu} - \hbar\omega)^2 + \gamma^2} \quad (23)$$

for the imaginary part  $\chi''(\omega)$  of the linear susceptibility  $\chi(\omega) = P(\omega)/E(\omega)$ . This quantity is directly proportional to the linear optical absorption spectrum. In Eq. (23),  $\mu_{\nu}$  is the optical matrix element in the two-particle basis, i.e.,

$$\mu_{\nu} = \sum_{\alpha\beta} \mu_{\alpha\beta} \Phi_{\alpha\beta}^{\nu}. \quad (24)$$

### 3.2 Photoluminescence

We exclusively consider steady-state photoluminescence which is a good approximation for sufficiently slowly varying carrier distribution. In that case, a good measure for the photoluminescence spectrum is given by

$$I_{\text{PL}}(\omega_q) = \frac{\partial}{\partial t} \langle \hat{b}_q^{\dagger} \hat{b}_q \rangle, \quad (25)$$

the rate of emitted photons[16]. In principle, direction and magnitude of  $\vec{q}$  determine emission direction and frequency; here, we limit ourselves to only one specific direction such that the scalar wave number  $q$  determines the frequency  $\omega_q = cq$ . Following a similar derivation as given in Refs. [19,20] for ordered semiconductor heterostructures, this quantity can be expressed as

$$I_{\text{PL}}(\omega_q) = \omega_q \sum_{\nu} \frac{|\mu_{\nu}|^2}{\epsilon_{\text{bg}}} \frac{\gamma S_{\nu}}{(\hbar\omega_q - \epsilon_{\nu})^2 + \gamma^2} \quad (26)$$

even for the disordered case. This formula is in close analogy to Eq. (23) and exhibits the same resonances as can be seen from the energy denominator. As in Eq. (23), we have used the low-density limit in which we have not taken into account the microscopic Coulomb scattering which would lead to a state- and frequency-dependent  $\gamma$ . [18] Thus, in reality the lineshape of the resonances is not a simple Lorentzian as is considered here. However, for sufficiently low densities and for the case of strong disorder, we expect the result to be dominated

by the inhomogeneous broadening such that the details of the homogeneous line shape are less important than for ordered semiconductors.

In general, the source term  $S_\nu$  contains true two-particle correlations of the form  $\langle \hat{e}^\dagger \hat{h}^\dagger \hat{h} \hat{e} \rangle$ . These correlations can either describe a Coulomb-correlated plasma beyond the pure Hartree-Fock limit[24] or additional bound excitons [18]. In the absence of any exciton formation, we find that these four-point quantities in the limit of a correlated plasma are given by [19,20]

$$S_\nu = \sum_{\alpha\beta} |\Phi_{\alpha\beta}^\nu|^2 f_\beta^e f_\alpha^h. \quad (27)$$

Note that this source term does not result from a Hartree-Fock factorization of the underlying correlation function [19,20]. Such an approach would yield a term which is non-diagonal in the indices  $\nu$  and  $\nu'$  characterizing the many-particle states and can lead to unphysical negative luminescence intensity. Only by considering in addition the correlations beyond Hartree-Fock these non-diagonal terms cancel and only one  $\nu$ -sum over pair states remains in Eq. (27). In general, the diagonal source term can contain contributions from both plasma and correlated bound excitons. In our situation of not too low temperatures it is known [19] that the latter can safely be neglected. Thus, the source term given in Eq. (27) describes the emission of a correlated electron-hole plasma and the formation of incoherent bound exciton populations is not taken into account.

A more complete theory should be based on a fully dynamic description including the relaxation on a microscopic level. As stated above, it is presently not feasible for us to numerically implement this approach for a strongly disordered interacting system. Thus, we assume stationary quasi-thermal distributions for the single-particle distributions  $f_\alpha^{e,h} = f_{\alpha\alpha}^{e,h}$  corresponding to the diagonal elements of the intra-band quantities  $f_{\alpha\beta}^h = \langle \hat{h}_\alpha^\dagger \hat{h}_\beta \rangle$  and  $f_{\alpha\beta}^e = \langle \hat{e}_\alpha^\dagger \hat{e}_\beta \rangle$ . The distributions are chosen such that a given density of carriers  $\rho = 10^{-3}$  per site is achieved.

## 4 Results and discussion

In the following, we analyze disorder-induced effects on semiconductor absorption and luminescence in the limit of small carrier densities. We concentrate, in particular, on situations where optically active exciton populations are not expected to play a crucial role. More specifically, we investigate both the direct- and indirect-based models for different carrier temperatures and various amounts of disorder by explicitly evaluating Eqs. (23) and (26).

#### 4.1 Absorption and photoluminescence spectra

For the direct- and indirect-based model, absorption and luminescence spectra are shown in Fig. 4 for a system of  $N = 10$  sites. The absorption spectrum of the ordered interaction-free case, Fig. 4a, shows four doubly degenerate transitions and two nondegenerate ones at the edges of the spectrum. The transitions at the energetically lowest interband energy difference (shown as a vertical line in Fig. 4 and taken as the zero of the energy scale) is indirect in  $k$ -space for the indirect-based model (indicated by a “c” in Fig. 3) and thus forbidden. In the ordered case, the only possible direct transitions connect states that are either at the top of the conduction band or at the bottom of the valence band. Since the corresponding carrier occupation is exponentially small, the luminescence signal is small as well (not seen in the figure where normalized data are shown). As a general trend, we observe that the central position of the luminescence spectrum is shifted towards lower energies compared to the symmetric absorption spectrum. This results from the carrier distributions which decreases with increasing electron and hole energy. Furthermore, the high-energy electron (high-energy hole) states in our present tight-binding model do not reflect states in a normal wide-band semiconductor. They might, however, be relevant for superlattices, polymers, or other narrow-band semiconductors.

Disorder leads to a violation of the  $k$ -selection rule in optical transitions. Thus, transitions that are forbidden in the ordered case may become allowed in the presence of disorder. This particularly applies to transitions between electron and hole states that form the lower and upper conduction and valence band extrema, respectively. This is seen in both the absorption and the luminescence spectrum, see Fig. 4b for the indirect-based model. Here, with disorder, the optical transitions extend down to photon energies corresponding to the smallest energetic separation across the gap. In the disordered situation, the red-shift of the center of mass of the luminescence spectrum relative to that of the absorption is much more pronounced than in the ordered situation.

The same trend is observed also if the Coulomb interaction is considered, see Fig. 4c-d. The difference with respect to the interaction-free case lies basically in the well-known fact that the interaction leads to an enhancement of the matrix elements of the energetically low transitions which is accompanied by a reduction for the high-energy ones. In the ordered case, a distinct excitonic resonance emerges while in the disordered case no single bound exciton can be identified, except perhaps for the very lowest transition close to -30 meV. For direct-based models, the situation is similar, except that the disorder-induced red shift of both spectra is less pronounced, since in this case, the energetically lowest interband transitions are allowed even in the ordered case.

### 4.1.1 The Stokes-Shift

The spectra of Fig. 4 are computed for one particular realization of the disorder. The configurationally averaged spectra, see Fig. 5, more clearly show the red shift of the luminescence spectrum with respect to the absorption spectrum, i.e., the disorder-induced Stokes shift. To quantitatively analyze the Stokes shift, we determine the energetic red-shift of the maximum of the luminescence spectrum with respect to the maximum of the absorption and denote it by  $\Delta E$ . One clearly observes that  $\Delta E$  is nonvanishing for both the direct- and indirect-based models; as shown in Fig. 5, it is slightly larger in the second case. It is also seen that the Stokes shift increases when lowering the temperature. A non-monotonous behavior at low temperatures is obtained if phonon induced relaxation and hopping are explicitly included in the description [1].

To complete the Stokes shift analysis, we present  $\Delta E$  of the configurationally averaged spectra as function of temperature in Fig. 6. Due to the quasi-thermal distribution of the carriers, the magnitude of the Stokes shift decreases with rising temperature. From Fig. 6a, we see that this effect is more pronounced for the indirect-based model. This is due to tailing of the spectra produced by the disorder-induced violation of the  $k$ -selection rule. These tails accommodate the low-energy carriers in both bands and lead to a larger weight at low photon energies in the luminescence spectra if compared to that of the direct-based model. The temperature dependence of the Stokes shift becomes more pronounced for elevated levels of the disorder. This is shown in Fig. 7 where  $\Delta E$  is presented as functions of disorder and temperature for the indirect-based model.

Figure 6b shows that the interaction tends to reduce the Stokes shift. This can be explained by observing that the interaction leads to an enhancement of the optical matrix elements for low-energy transitions for both absorption and luminescence. Thus, even in the absence of disorder, the absorption spectrum is energetically more concentrated at low energies such that additional disorder is less effective compared to the interaction-free case.

In order to judge whether the small number of sites is a severe limitation for the present study, we compare  $\Delta E$  results of  $N = 10$  and  $N = 30$  sites in Fig. 6c. This indicates that  $N = 10$  sites provides fairly converged results since the Stokes shift only moderately depends on  $N$ . Fig. 6d demonstrates the convergence of the results with respect to increasing number of realizations used in the configurational average. Once again, a good convergence is observed already with  $10^4$  realizations, used in most of the computations.

#### 4.1.2 Structure of the spectra

As seen in Fig. 4, the spectrum for a single realization consists of a very broad distribution of peaks of different height. In order to investigate to what extent our procedure of configurational averaging is meaningful, we compare it to an alternative approach. Therefore, we pick the spectral maxima for each configuration as the most relevant single piece of information and study their distribution. In Fig. 8, the distributions of the luminescence and the absorption maxima are presented for  $T = 10\text{K}$  and  $W/J = 4$  showing data for 10 000 disorder realizations. The maxima of the absorption spectra are denoted by squares, while those of the luminescence spectra are given by  $+$ . The center of mass of each distribution is indicated by the corresponding large symbol.

These averages of the maxima result in identical qualitative trends for the Stokes shift as the maxima of the averages in Fig. 4, supporting the validity of the analysis of the spectra in terms of configurational averages.

In addition to the two sets of distributions in Fig. 8, we also show the height of the absorption for every realization at that energy where the luminescence spectrum has its maximum ( $x$ ), and vice-versa ( $*$ ). Both types of data taken from luminescence spectra ( $+$  and  $x$ ) show a decreasing trend with increasing energy. Since this is not the case with data taken from absorption spectra (square and  $*$ ) this gives an additional justification for the definition of the disorder-induced Stokes shift.

In Fig. 9 the same distributions are shown, however, now at a higher temperature of  $T = 77\text{K}$ . In this case the quasi-thermal distributions are more extended in energy, leading to a less pronounced dependence of the height of the maxima of the luminescence spectra on the emission energy. The magnitude of the Stokes shift is reduced in agreement with the data in Fig. 7.

#### 4.1.3 Disorder-induced convergence of spectra for direct- and indirect-based models

Our computations show that the luminescence spectra for direct- and indirect-based models are different. This is most pronounced at low temperature, see Fig. 10, where averaged spectra for low ( $T = 5\text{K}$ ) and higher temperature ( $T = 30\text{K}$ ) are presented. Evidently, if disorder is increased, the spectra are expected to converge for both cases since band structure effects are expected to become unimportant for dominantly disordered systems. This trend is verified by Fig. 10. Nevertheless, we find it remarkable that even for relatively large disorder ( $W/J = 16$ ) the spectra still differ clearly from each other. This difference is more pronounced at low temperature.

The luminescence spectra of Fig. 10 show a double-peaked structure in the

low-temperature data for the indirect-based models. To understand this feature, one has to realize that the spectra cover the total bandwidth of the tight-binding model. In particular, the double-peaked structure follows from: (i) transitions located close to the lowest energetic separation of electron and hole states and (ii) to transitions of type (a) and energetically higher ones indicated in Fig. 3, weighted by the carrier occupations. However, our tight-binding model describes real semiconductors adequately only in a small energetic window close to the fundamental gap. Energetically higher transitions have no direct correspondence to those in real semiconductors with their much larger band widths. Therefore, the double-peak structure seen at low temperatures should be taken as an artifact of the model, if one is interested in modeling a conventional wide-band semiconductor. On the other hand, this structure might correspond to realistic features for such systems that are characterized by small band widths. Examples include minibands in semiconductor superlattices or organic polymers, provided the underlying ordered system is an indirect semiconductor.

#### 4.2 *Thermodynamic Relation*

Since the radiative recombination typically takes place on a nanosecond time-scale, it might be tempting to calculate the steady-state luminescence spectrum under the assumption that the light-matter interaction acts as a weak perturbation and to assume thermodynamic quasi-equilibrium distributions for the photoexcited carrier system, due to e.g. fast phonon scattering. In this strict thermodynamic limit it is possible to derive a thermodynamic relation between photoluminescence and absorption [25]

$$I_{\text{TD-PL}}(\omega) = g(\omega) \alpha(\omega), \quad (28)$$

where  $g(\omega)$  is given by a Bose-Einstein distribution.

For ordered semiconductors, however, it is well known and understood that this approximation fails at the 1s-exciton resonance. Several recent experiments [18,26,27] demonstrate that the luminescence at the 1s-exciton resonance strongly violates Eq. (28) even after all excitation transients have been completely equilibrated. In this case, the nonthermal behavior originates from the strong depletion of optically active excitons implying that photoluminescence is not a weak perturbation for exciton distributions [17] and that, consequently, the thermodynamic arguments cannot be used. Even though the single particle distributions may be close to Fermi-Dirac distributions, the two-particle excitonic distributions can be very nonthermal and especially the 1s-distribution can exhibit considerable hole-burning. Thus, the photoluminescence at the 1s-exciton resonance is in many situations dominated by

correlated plasma contributions rather than exciton populations. The result is a nonthermal 1s luminescence for nearly disorderless systems [18]. However, it is also known that Eq. (28) typically remains valid for photon energies corresponding to the continuum states when the semiconductor carriers have reached a quasi-equilibrium after the excitation. Thus, for elevated carrier densities and temperatures as they occur e.g. under lasing conditions when the Coulomb interaction is strongly screened and the excitonic resonance is bleached out, Eq. (28) can be safely used to calculate luminescence from absorption spectra.

Our goal in the following section is to investigate whether the thermodynamic relation can be recovered even for the correlated-plasma emission when the system has a considerable amount of disorder. Since we only study luminescence from systems with dilute carrier densities we can replace the Bose-Einstein distribution  $g(\omega)$  by a Boltzmann distribution  $g(\omega) = N_g e^{-\hbar\omega/k_B T}$  with a suitable normalization constant  $N_g$ .

To determine the nonthermal aspects of the luminescence spectrum, we apply the following procedure: i) we first determine an effective temperature  $T_{\text{eff}}$  by fitting  $g(\omega) = N_g e^{-\hbar\omega/k_B T_{\text{eff}}}$  to the continuum part of the ratio  $I_{\text{PL}}(\omega)/\alpha(\omega)$ , where Eq. (28) is known to be valid. ii) After this, we use Eq. (28) to predict the thermodynamic value,  $I_{\text{TD-PL}}(\omega_1) = g(\omega_1) \alpha(\omega_1)$ , for the lowest excitonic resonance at the frequency  $\omega_1$ . iii) This allows us to quantify the degree of nonthermal behavior via a  $\beta$  factor,

$$\beta = \frac{I_{\text{PL}}(\omega_1)}{I_{\text{TD-PL}}(\omega_1)}, \quad (29)$$

which has been determined according to Schnabel et al. [26]. In other words, the  $\beta$  factor describes how strongly the calculated luminescence  $I_{\text{PL}}(\omega_1)$  is suppressed compared to the expected thermodynamic value  $I_{\text{TD-PL}}(\omega_1)$  as obtained from the absorption spectrum via Eq. (28). A strict thermodynamic value is observed when  $\beta = 1$  while  $\beta \ll 1$  indicates a strong violation of the thermodynamic relation.

This  $\beta$  analysis reveals generic disorder dependent features which are illustrated in Fig. 11 where the upper row shows the actual luminescence spectra (filled areas) in comparison with the thermodynamic spectrum (dashed line) constructed via Eq. (28). The lower row compares the fitted Maxwell distribution  $g(\omega) = e^{-\hbar/k_B T_{\text{eff}}}$  with the actual ratio  $I_{\text{PL}}(\omega)/\alpha(\omega)$  for the corresponding spectra. These computations were performed for a carrier temperature of 77 K and three different levels of disorder: weak ( $W/J = 1$ , left column), intermediate ( $W/J = 8$ , middle column), and strong disorder ( $W/J = 16$ , right column). All spectra are evaluated using 10 sites and averaging over  $10^4$  realizations is applied. For the nearly disorderless case ( $W/J = 1$ ), we find  $\beta = 0.46$  in-



dicating a clear violation of the thermodynamic relation. When the disorder amplitude is increased,  $\beta$  starts to approach unity. For the largest disorder used, we find  $\beta = 0.93$ , which shows that an increased amount of disorder helps to recover the thermodynamic relation even for the excitonic plasma luminescence. In this case, the actual and the thermodynamic luminescence spectra are very close to each other.

The role of disorder can be intuitively understood if we consider that the excitonic luminescence peak consists of a quasi-continuous distribution of energies for the high disorder case while only a single discrete excitonic energy is present for the low disorder case. Since the strongly disordered emission peaks are weighted thermodynamically in the total luminescence, a fully thermodynamic relation is approached as the disorder increases.

Figure 12 shows  $\beta$  (solid line) as a function of disorder for a lattice temperature of  $T = 77$  K (upper frame), and  $T = 20$  K (lower frame); the inset displays the corresponding  $T_{\text{eff}}$ . We observe that for 20 K carriers, the lowest  $\beta$  lies below 0.04 and increases monotonously with increasing disorder. Otherwise, similar qualitative behavior is observed as for 77 K. For both 20 K and 77 K, the disorder averaged spectra have noise. As a result,  $\beta$  has error bars which increase for elevated level of disorder; the error is indicated by the shaded areas. The inset displays the effective temperature fitted from the luminescence tail.

Actual experiments have only a limited access to the quantities determining the carrier system, e.g., luminescence and absorption spectra can be determined while exact carrier distributions remain usually unknown. The  $\beta$ -analysis procedure applied above only assumes that carrier distributions are in quasi equilibrium such that one can conveniently use the same approach for an experimental analysis. As an additional theory feature, we can study how well the determined effective temperature corresponds to the actual carrier temperature. We observe that the effective temperature is always higher than the nominal carrier temperature used in the computations, which is in agreement with previous findings for ordered semiconductors.

### 4.3 *The radiative lifetime distribution*

If nonradiative recombination of electrons and holes can be neglected, the area under the stationary luminescence spectra directly reflects the radiative lifetime  $\tau$  of the electron-hole system, i.e., the lifetime is simply inversely proportional to the area under the total spectrum. Thus, each spectrum for a given realization defines a single  $\tau$  and the lifetimes calculated for many realizations define a distribution of a certain shape. In practice, the lifetime

can be calculated from Eq. (26) as  $\tau^{-1} = \int d\omega I_{\text{PL}}(\omega)$  yielding the relation

$$\frac{1}{\tau} \sim \sum_{\nu} |\mu_{\nu}^2| S_{\nu} \varepsilon_{\nu}. \quad (30)$$

For both the direct- and the indirect-based models we show such lifetime distributions for the non-interacting and the interacting case as function of temperature for a weakly and strongly disordered situation in Figs. 13 and 14.

If the disorder is weak, i.e., smaller than the exciton binding energy ( $W/J = 1$ ), the distributions for both non-interacting and interacting cases follow a log-normal form

$$\mathcal{P}(\log \tau) \propto \exp \left\{ -\log(\tau/\tau_0)^2 / 2\sigma^2 \right\}. \quad (31)$$

For the indirect-based model (upper panel in Fig. 13), the distributions shift towards longer (shorter) times for the interacting (non-interacting) situation with increasing temperature. On the other hand, for the direct-based model both sets of distributions follow the same trend as function of temperature. The distributions become narrower on a logarithmic scale with increasing temperature.

The interpretation is as follows: in the non-interacting case, the carriers occupy higher states for increasing temperature. In the indirect-based model, transitions between these states have larger matrix elements compared to those between the energetically low-lying states due to the still dominant indirect nature at weak disorder. Therefore, with increasing temperature the emission becomes increasingly more efficient, i.e., the lifetime decreases. This effect is overcompensated by the Coulomb interaction. In this case, already at low temperature, i.e., when low-energy transitions dominate, the interaction increases the otherwise small optical matrix elements leading to an enhanced emission and short lifetimes. With increasing temperature energetically higher transitions become involved which are characterized by a smaller Coulomb-induced enhancement. Thus, their weight decreases if compared to the low-temperature case. At high temperature, the distributions converge due to a smearing out of the distributions over a large energetic region and interaction is no longer important.

For direct-based models, also for the non-interacting case the low-energy transitions dominate the weight of the spectrum at low temperatures, thus both sets of distributions behave in a similar way. The temperature dependence of the interacting case is slightly more pronounced.

Finally, at the end of this discussion of the lifetime we would like to make a connection with different but related context. For relatively large disorder

( $W/J = 16$ ), larger than the exciton binding energy, both sets of distributions become quite similar to each other, see Fig. 14. They both shift towards larger lifetimes with increasing temperature. However, for low temperatures, they deviate from a log-normal distribution. At the lowest temperature ( $T = 5$  K), only a monotonously decreasing  $\mathcal{P}$  is observed as function of increasing  $\tau$ . The explanation lies in the fact that there is a cut-off at a minimum lifetime which is defined by the spatially direct transition within a single isolated two-level system representing a site. Its matrix element is simply given by the model parameter  $\mu_0$ . Furthermore, the log-log plot presented in the lower panel in Fig. 14 shows that for strong disorder and low temperatures the lifetime distribution follows an overall power-law dependence with an exponent close to unity.

The above behavior of log-normal lifetime distribution for high temperatures and low disorder and power-law distribution for sufficiently low temperatures and strong disorder resembles the behavior seen in other disordered systems. In general terms, an electronic excitation may decay if the system is coupled to the outside, i.e., if it is an open system. This decay manifests itself in a homogeneous broadening of the sharp spectral line of the electronic excitation in a closed system. In our system, however, this homogeneous broadening is neither described by the Hamiltonian [28], nor would it be possible to be seen, since our spectrum is dominantly inhomogeneously broadened. Nevertheless, we are able to determine the radiative lifetime  $\tau$  by integrating over the luminescence spectrum, since we are considering a stationary situation.

The lifetime is related to the coupling of the electronic states that describe the excitation to the environment. So far, lifetime has been mostly discussed in the context of electronic transport [29,30,31]. In that case, it is the amplitude of the wave function at the position where the leads are attached to a system which determine the lifetime. In our case, the lifetime is determined by the optical dipole matrix element  $\mu_\lambda$ . From the Elliott formula, Eq. (26), we see that the lifetime distribution (or its inverse as recombination rate) follows the distribution of  $S_\nu$ , Eq. (27), and through this quantity it is also based dominantly on the wave function components. It is known for the case of weakly disordered systems that the wave function components obey log-normal distribution in quasi-one dimensional systems which is applicable here.[29] Moreover, it has recently been shown [30,32] that resonance width distributions in diffusive systems show a crossover behavior between a log-normal and a power-law behavior. However, the exponent is different from the one obtained in the present calculation, but the discussion in this field are not yet settled. There are several works in the literature where power-law distributions of power equal to one are obtained.[31,33]

We would like to mention, that the appearance of log-normal behavior of the recombination times resembles also the hierarchical lifetime structure seen

in spin-glass systems [31,34,35]. These consist of coupled two-level systems similarly to the disordered model of a semiconductor presented here. Presently, we do not see a link between these two fields but apparently an unusual analogy can be detected which deserves further investigation.

The observation that the distributions for both the interacting and non-interacting cases show a similar behavior for large disorder demonstrates the fact that Coulomb interaction becomes less important with increasing disorder. Roughly speaking, for the short-range disorder potentials fluctuating on an energy scale on the order of the exciton binding energy the dominant features of the luminescence spectra are determined by disorder. On the other hand, interaction-induced features will be clearly visible even for large disorder if the length scale of the disorder potential is larger than the exciton Bohr radius. This situation will be studied in a forthcoming paper.

## 5 Conclusions

As a first step towards a fully microscopic theory of luminescence in strongly disordered semiconductors, we have studied a two-band tight-binding model including Coulomb interaction and diagonal short-range disorder of arbitrary strength. Both absorption spectra and luminescence spectra have been calculated from modified Elliott formulas, which include the electron-hole pair states in the presence of disorder and the correlated-plasma source term for luminescence. The calculations are based on a direct diagonalization of the many-particle Hamiltonian.[36] Certain simplifications have been made and discussed in order to obtain a computationally feasible description of the strongly disordered, interacting semiconductor. We believe that for the present case study these simplifications are justified. We have exclusively considered stationary luminescence and have ignored nonradiative processes.

In its present state, our approach cannot directly be applied to those experimental data where the phonon-assisted dynamics is known to take place on a time scale longer than that of the recombination. This is the case for low temperatures, see, e.g., [1]. On the other hand, we have shown that a description of radiative recombination in disordered semiconductors is feasible treating disorder and many-particle interactions on equal footing without using special model assumptions for bound-excitonic vs. plasma recombination.

In particular, we have in detail studied the influence of disorder, Coulomb interaction, direct- or indirect-based models, and temperature on the disorder-induced Stokes shift and the radiative lifetime distribution. The results and their interpretation are applicable to stationary luminescence measurements of strongly disordered semiconductors including polymers [37] and superlat-

ices [38] for not too low temperatures and for quasi-stationary situations where optically active exciton populations are negligible. The cross-over from the low-temperature to the high-temperature regime depends on details of the model, such as density of states and degree of disorder.

Time-resolved measurements or measurements on systems that are characterized by slow relaxation processes due to hopping events are outside the scope of this work, i.e., the low-temperature data of this calculation should be taken as a case study of our model system only. In realistic systems at extremely low temperatures, hopping processes may become extremely slow such that the assumption of quasi-thermal carrier distributions can no longer be justified. For higher temperatures, on the other hand, the observed trends can give support to an interpretation of stationary luminescence spectra of strongly disordered semiconductors.

## References

- [1] S. D. Baranovskii, R. Eichmann, and P. Thomas, *Phys. Rev. B.* **58**, 13081 (1998).
- [2] R. Zimmermann and E. Runge, *phys. stat. sol. (a)* **164**, 511 (1997).
- [3] E.M. Daly, T.J. Glynn, J.D. Lambkin, L. Considine, and S. Walsh, *Phys. Rev. B.* **52**, 4696 (1995).
- [4] S.T. Davey, E.G. Scott, B. Wakefield, and G.J. Davies, *Semicond. Sci. Technol.* **3**, 365 (1988).
- [5] M.S. Skolnick, P.R. Tapster, S.J. Bass, A.D. Pitt, N. Apsley, and S.P. Aldred, *Semicond. Sci. Technol.* **1**, 29 (1986).
- [6] R. Stachowitz, M. Schubert, and W. Fuhs, *J. of Non-Cryst. Sol.* **190**, 227-230 (1998).
- [7] H. Grüning, K. Koháry, S.D. Baranovskii, O. Rubel, P.J. Klar, A. Ramakrishnan, G. Ebbinghaus, P. Thomas, W. Heimbrodt, W. Stolz, and W. Rühle, *phys. stat. sol. (c)* **1**, 109 (2004).
- [8] A. Zukauskas, K. Kazlauskas, G. Tamulaitis, M. A. Khan, J. W. Yang, J. Zhang, G. Simin, M. S. Shur, and R. Gaska, *phys. stat. sol. (c)* **0**, 2737 (2003).
- [9] B. Dal Don, K. Koháry, E. Tsitsishvili, S.D. Baranovskii, P. Thomas, and H. Kalt, *Phys. Rev. B.* **69**, 045318 (2004).
- [10] B.I. Shklovskii, H. Fritzsche, and S.D. Baranovskii, *Phys. Rev. Lett.* **62**, 2989 (1989).

- [11] O. Rubel, S.D. Baranovskii, K. Hantke, J.D. Heber, J. Koch, P. Thomas, W. Stolz, W.W. Rühle, J.M. Marshall, *J. Optoelectronics and Advanced Materials* **7**, 115 (2005).
- [12] F. Boullitrop and D. J. Dunstan, *Phys. Rev. B* **28**, 5923 (1983).
- [13] J. Singh, T. Aoki, K. Shimakawa, *Phil. Mag. B* **82**, 855 (2002).
- [14] Jai Singh and I.-K. Oh, *J. Appl. Phys.* **97**, 063516 (2005).
- [15] M. Kira, F. Jahnke, S. W. Koch, *Phys. Rev. Lett.* **81**, 3263 (1998).
- [16] M. Kira, F. Jahnke, W. Hoyer, and S. W. Koch, *Prog. Quant. Electr.* **23**, 189 (1999).
- [17] M. Kira, W. Hoyer, T. Stroucken, and S. W. Koch, *Phys. Rev. Lett.* **87**, 176401 (2001).
- [18] S. Chatterjee, C. Ell, S. Mosor, G. Khitrova, H.M. Gibbs, W. Hoyer, M. Kira, S. W. Koch, J. Prineas, and H. Stolz, *Phys. Rev. Lett.* **92**, 067402 (2004).
- [19] W. Hoyer, M. Kira, and S. W. Koch, *Phys. Rev. B* **67**, 1551131 (2003).
- [20] W. Hoyer, M. Kira, and S. W. Koch, Cluster Expansion in Semiconductor Quantum Optics, in *Nonequilibrium Physics at Short Time Scales* ed. by K. Morawetz (Springer, Berlin, 2004).
- [21] H. Haug and S. W. Koch, *Quantum Theory of the Optical and Electronic Properties of Semiconductors*, 4th ed. (World Scientific, Singapore, 2004).
- [22] L. Bányai, I. Galbraith, C. Ell, H. Haug, *Phys. Rev.* **B36**, 6099 (1987).
- [23] The box distribution is usual choice well known in the literature of the Anderson model of disorder-induced localization, see, e.g., B. Kramer and A. MacKinnon, *Rep. Prog. Phys.* **56** 1469 (1993).
- [24] W. Hoyer, M. Kira, and S. W. Koch, *phys. stat. sol. (b)*, **234**, 195 (2002).
- [25] R. Zimmerman, *Many-Particle Theory of Highly Excited Semiconductors* (Teubner, Leipzig, 1988).
- [26] R.F. Schnabel, R. Zimmermann, D. Bimberg, H. Nickel, R. Lösch, and W. Schlapp, *Phys. Rev. B* **46**, 9873 (1992).
- [27] J. Szczytko, L. Kappei, J. Berney, F. Morier-Genoud, M. T. Portella-Oberli, and B. Deveaud, *Phys. Rev. Lett.* **93**, 137401 (2004).
- [28] More precisely, it is described with the phenomenological model parameter  $\gamma$ .
- [29] A. D. Mirlin, *Phys. Rep.* **326**, 259 (2000).
- [30] A. Ossipov, T. Kottos, and T. Geisel, *Europhys. Lett.* **62**, 719 (2003).
- [31] M. Terraneo and I. Guarneri, *Eur. Phys. J. B* **18**, 303 (2000).
- [32] M. Titov and Y. V. Fyodorov, *Phys. Rev. B* **61**, R2444 (2000).

- [33] F. A. Pinheiro, M. Rusek, A. Orlowski, and B. A. van Tiggelen, Phys. Rev. E **69**, 026605 (2004); S. Wimberger, A. Krug, and A. Buchleitner, Phys. Rev. Lett. **89**, 263601 (2002)
- [34] G. Casati, G. Maspero, and D. L. Shepelyansky, Phys. Rev. Lett. **82**, 524 (1999).
- [35] B. Castaing and J. Souletie, J. Phys. I **1**, 403 (1991).
- [36] We have also calculated luminescence spectra dynamically using the equation-of-motion approach; the results (not shown here) give identical results, but with appreciably larger numerical effort.
- [37] *Semiconducting Polymers*, ed. by G. Hadziionou and P. F. van Hutten (Springer, Berlin, 2000).
- [38] A. J. Chiquito, F. Lanciotti Jr., P. S. Pizani, and M. G. de Souza, Phys. Rev. B **69**, 113310 (2004).

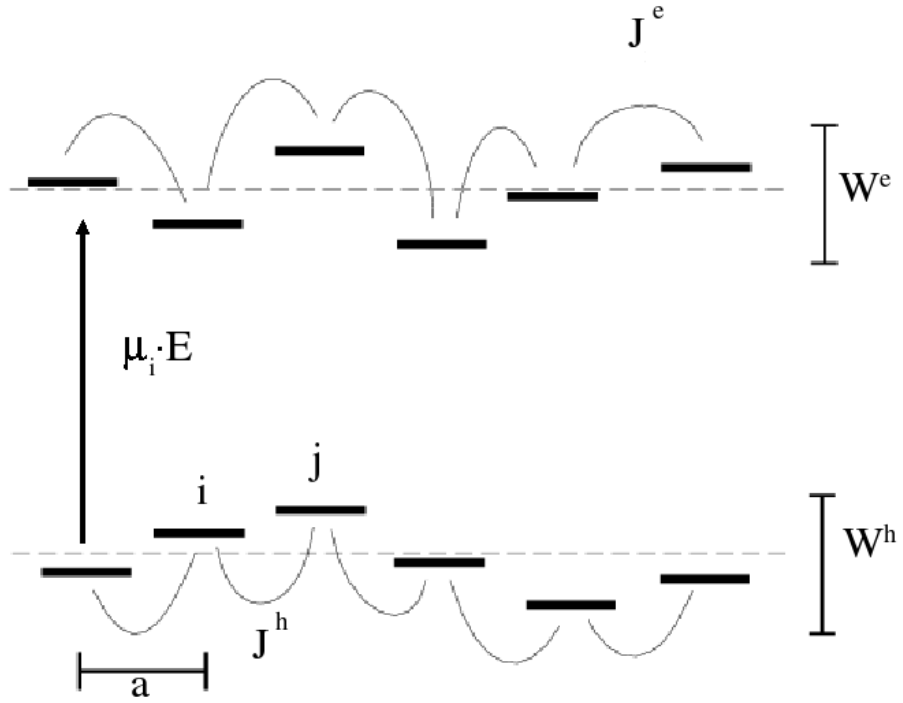


Fig. 1. Pictorial representation of the tight-binding model. The energies of the isolated sites are distributed over a disorder width  $W^e$  and  $W^h$  and coupled to the nearest neighbors via couplings  $J^e$  and  $J^h$ . The local excitation at site  $i$  with matrix element  $\mu_i$  generates a polarization. The lattice constant is  $a$ .

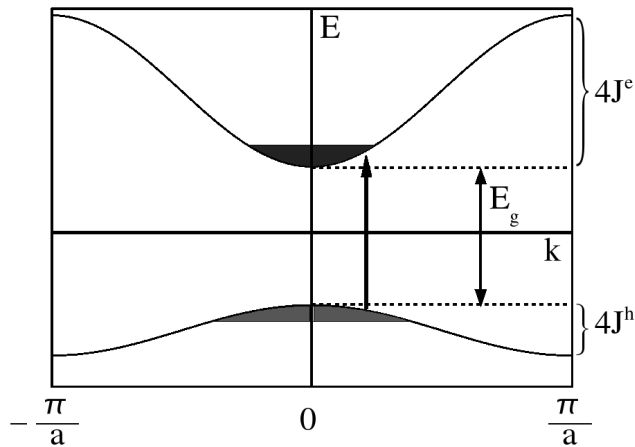


Fig. 2. Band structure of the ordered system representing a direct semiconductor. The shaded areas indicate occupied states due to pumping in the conduction and valence bands. The arrow indicates an allowed optical transition in a single-particle picture.  $E_g$  denotes the band gap in the ordered case.



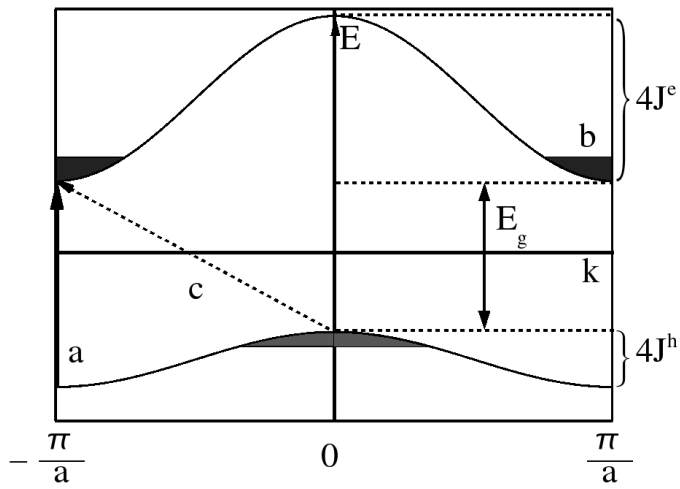


Fig. 3. Band structure of the ordered system representing an indirect semiconductor. The shaded areas indicate occupied states due to pumping in the conduction and valence bands. The solid arrow indicates the lowest allowed optical transition connecting the minimum of the valence band (a) with the minimum of the conduction band (b) in the single-particle picture. The dashed arrow denotes an indirect transition which is forbidden in the ordered case. It becomes partly allowed if disorder is introduced.  $E_g$  denotes the band gap in the ordered case.

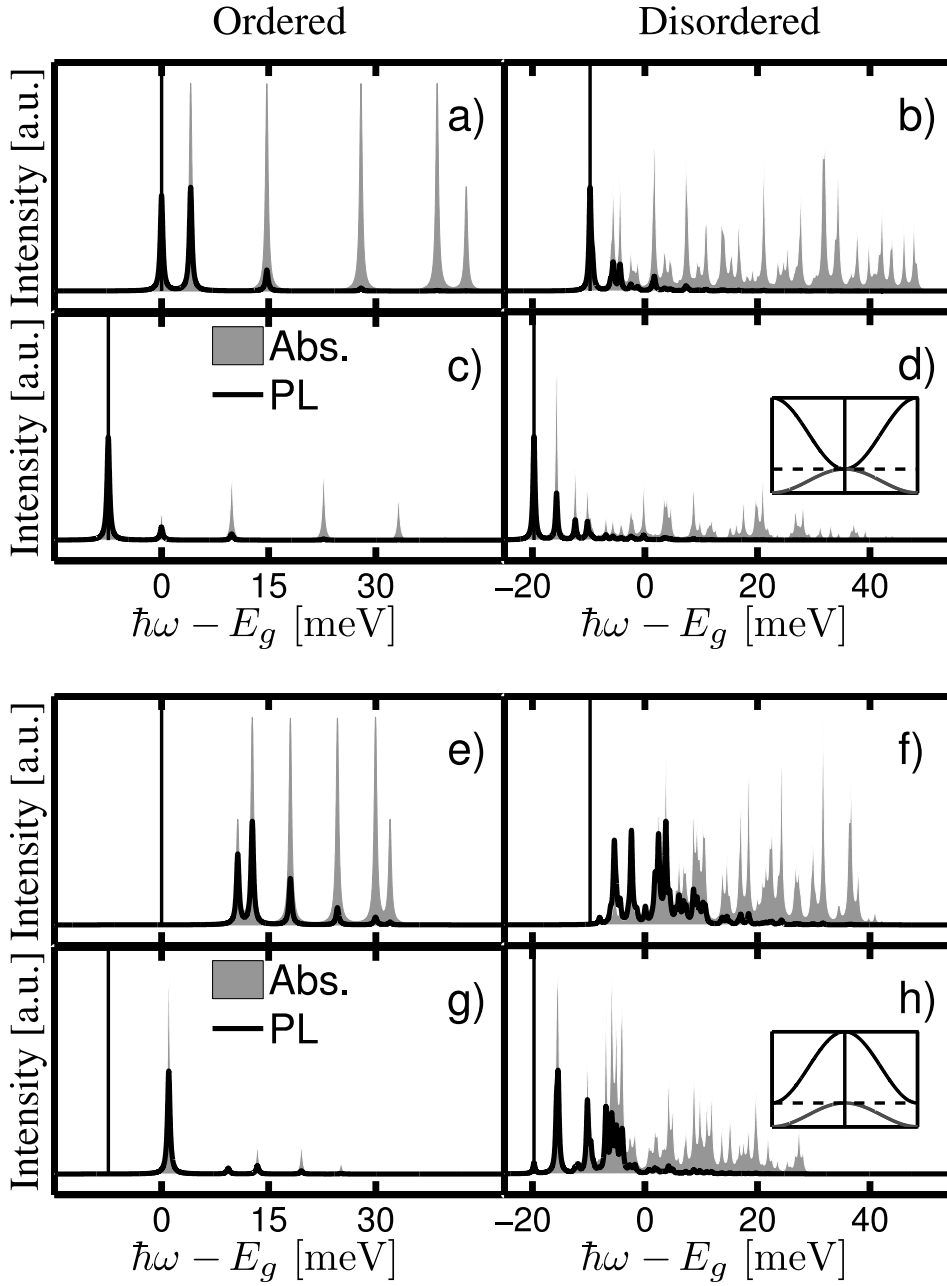


Fig. 4. Optical absorption (shaded areas) and luminescence (solid lines) spectra for ordered and disordered non-interacting and interacting direct- (upper panel) and indirect- (lower panel) based models. Insets give the band structure of these two ordered cases, showing that the zero of the photon energy has been chosen to coincide with the minimal state-energy separation, see Figs. 2 and 3. The thin vertical line indicates the smallest energy separation for any given case. a), e) Absorption and luminescence spectra for an ordered non-interacting model. The quasi-discrete spectra result from the system being composed from only  $N = 10$  sites. b), f) The same situation, but uncorrelated disorder is introduced ( $W = 4J$ ). c), g) Spectra of the ordered interacting model. d), h) Spectra of the disordered interacting model. Spectra for a single realization of disorder are shown. Note that due to the k-selection rule the optical transitions start at higher energies than the minimal energy separation in the ordered indirect-based models, e) and g), while disorder tends to close this gap, f) and h).

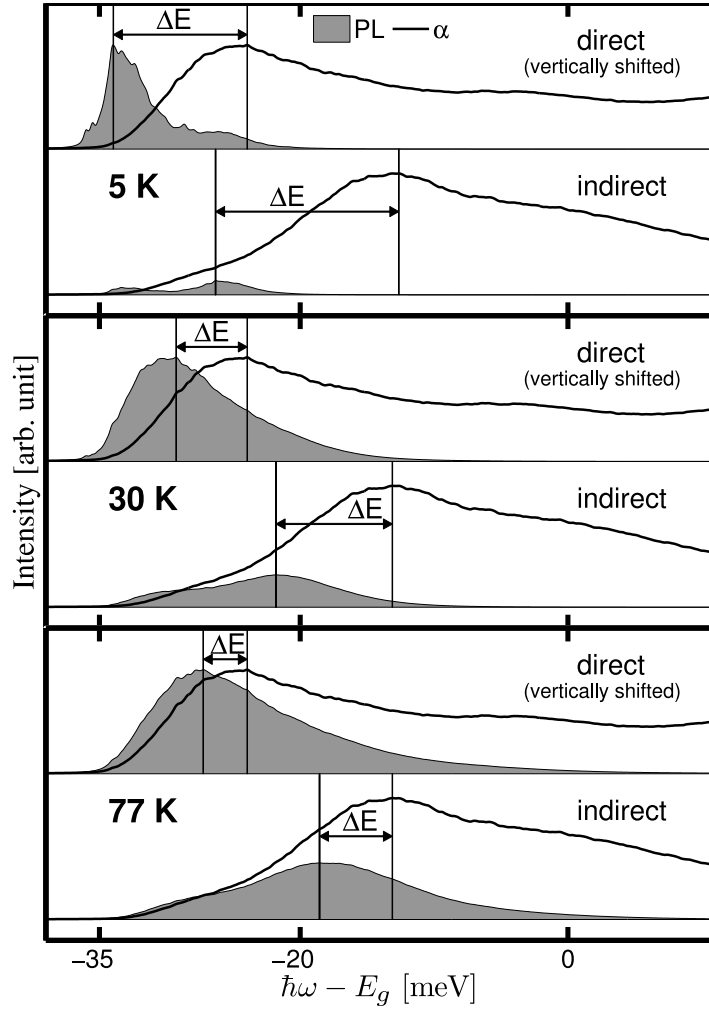


Fig. 5. Spectra for disordered interacting systems, based on both direct and indirect models. Configurational averages are shown.  $\Delta E$  indicated the Stokes shifts. The disorder parameter is  $W = 4J$ .

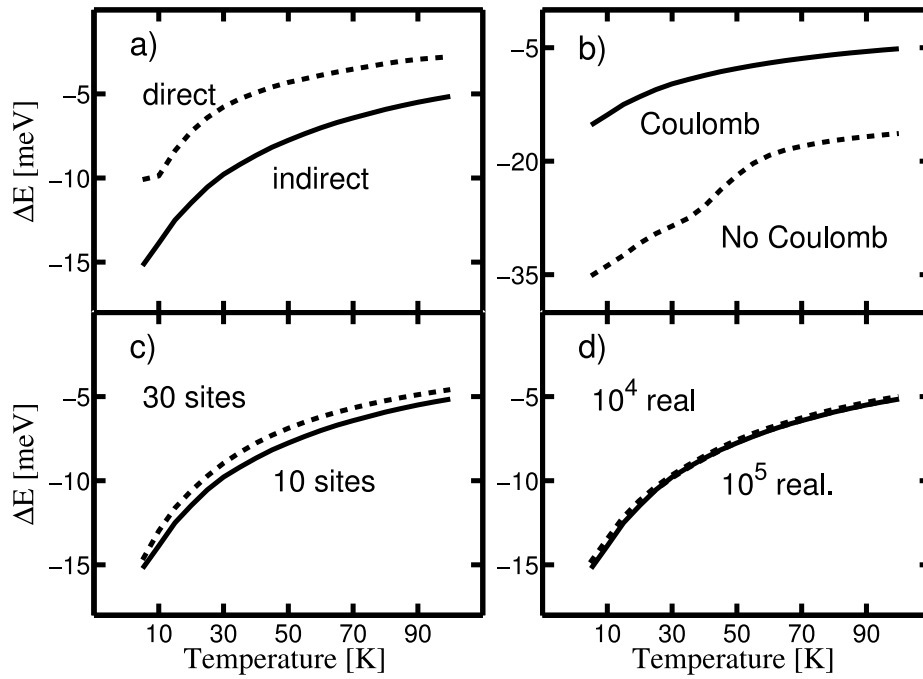


Fig. 6. Stokes shift for disordered models,  $W = 4J$ , as function of temperature. a) Compares direct- and indirect-based models. b) Shows the influence of the Coulomb interaction and c) the influence of the number of sites  $N$ . d) Demonstrates convergence with respect to the number of realizations. b), c), and d) correspond to the indirect-based model.

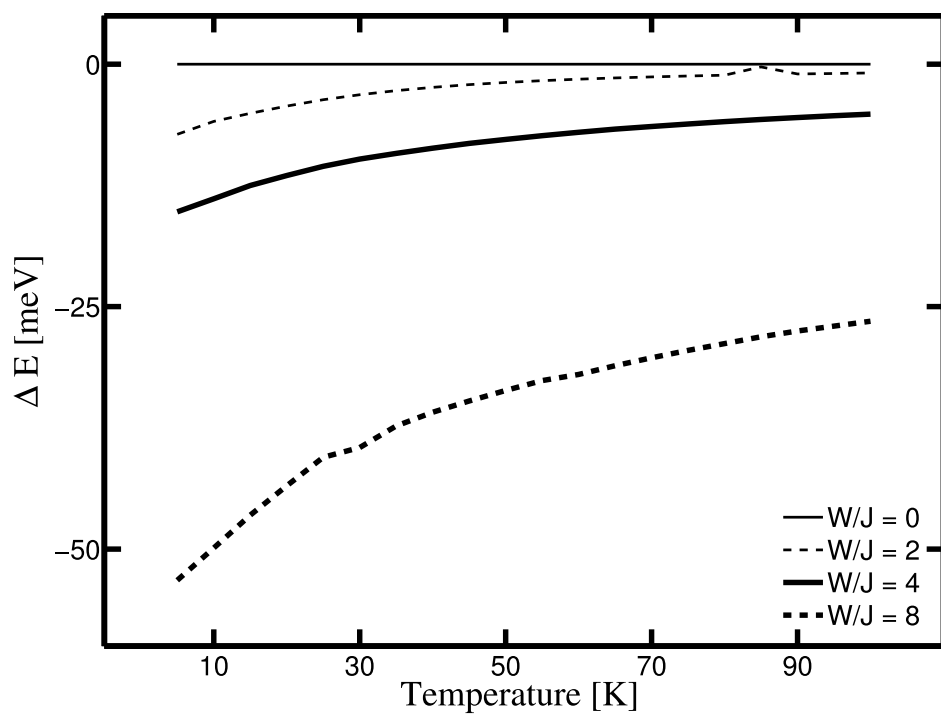


Fig. 7. The Stokes shift as function of temperature for different disorder parameters  $W$ . Every point corresponds to a Stokes shift obtained from the maxima of the configurationally averaged spectra.

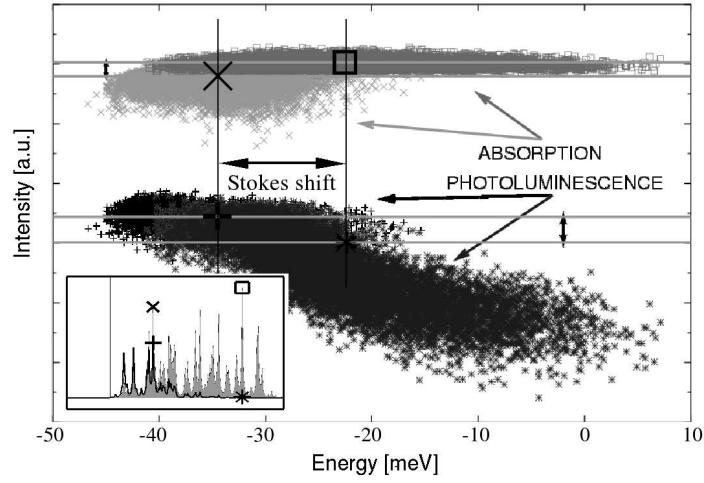


Fig. 8. Distribution of the maxima of the absorption and luminescence spectra for  $10^4$  realizations. Here  $T = 10\text{K}$ ,  $W = 4J$ . Squares: Distribution of the maxima of the absorption spectra. +: Distribution of the maxima of the luminescence spectra. For every square the height of the corresponding luminescence spectrum at the same energy is given by a \*. For every + the height of the corresponding absorption spectrum is given by an x. Big symbols denote center of mass of the corresponding cloud.

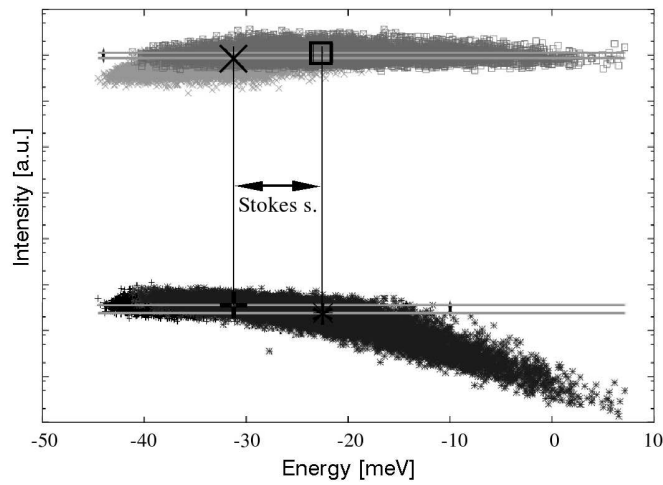


Fig. 9. Same as Fig 8, but  $T = 77\text{K}$ .

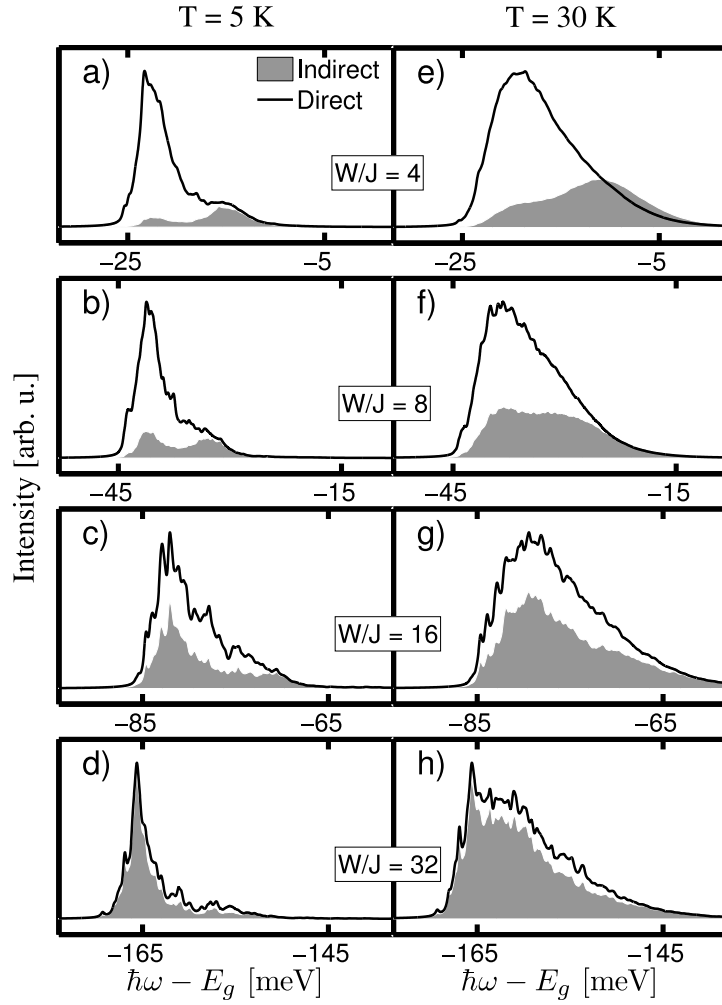


Fig. 10. Comparison of luminescence spectra for direct and indirect based models for various disorder  $W/J$  and for  $T = 5\text{K}$  and  $T = 30\text{K}$ . Filled areas: indirect based models. Full lines: direct-based models. Configurationally averaged data are shown.

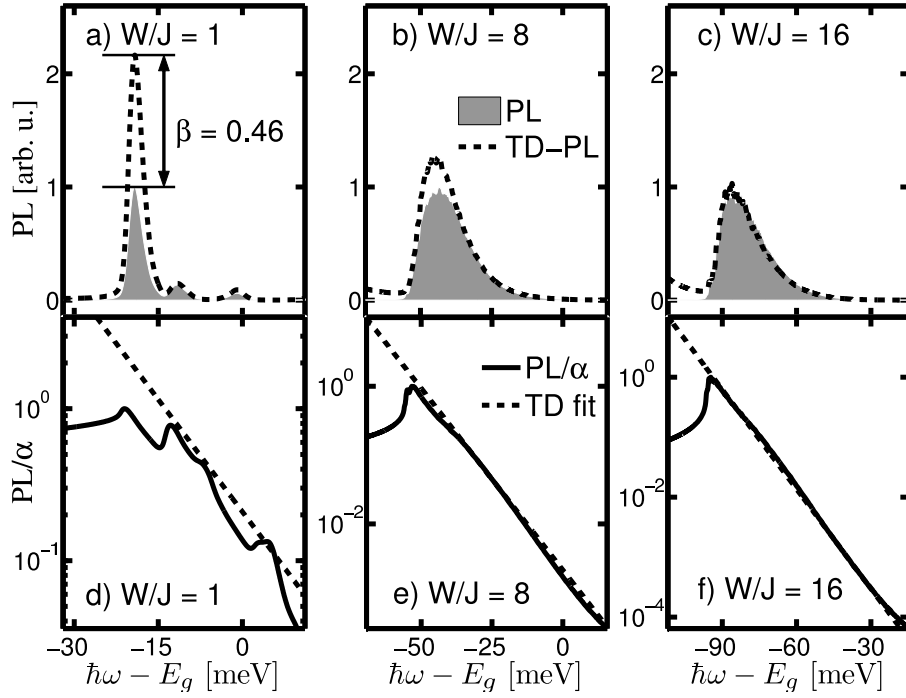


Fig. 11. Deviation of the luminescence spectra from the thermodynamical relation. The calculated luminescence spectra (filled area) are compared with the luminescence derived from absorption  $\alpha$  using the thermodynamic relation (dashed line) on a linear scale for  $W/J=1, 8, 16$  in the upper row. In the lower row the  $PL/\alpha$  ratio (solid line) is fitted by the thermal line (dashed line) on a semi-log scale.



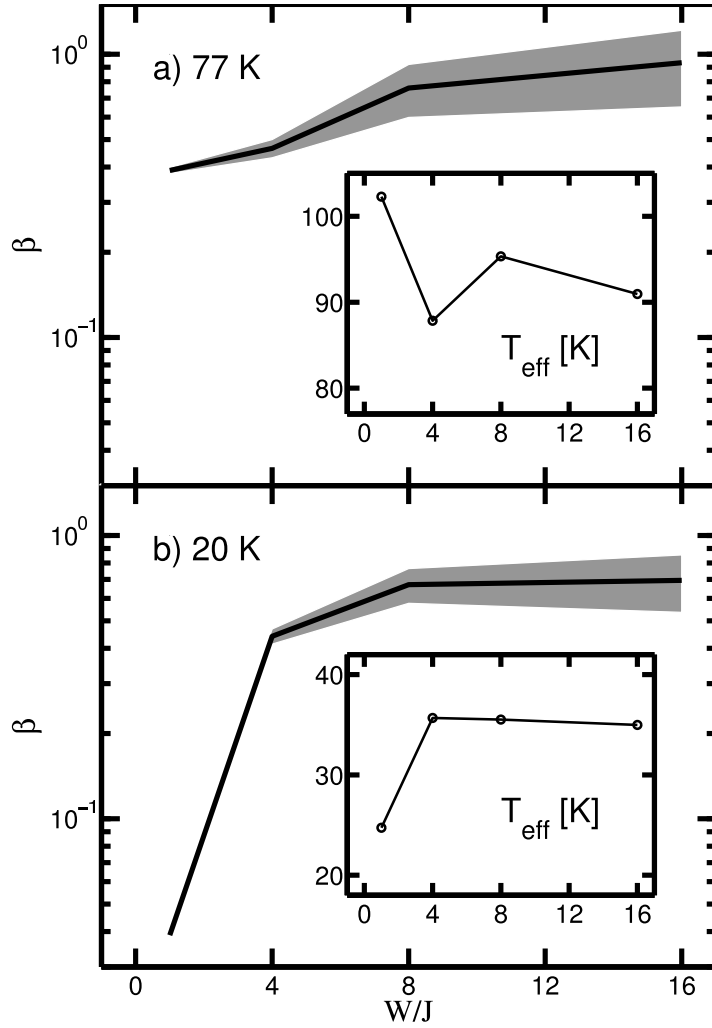


Fig. 12. The dependence of the amount of deviation from the thermal value,  $\beta$ , as function of disorder (solid line). The error of the fit is also denoted (shaded area). Shown are data for  $T = 77$ K (upper figure) and  $T = 20$ K (lower figure). The insets show how  $T_{\text{eff}}$  changes with increasing disorder.

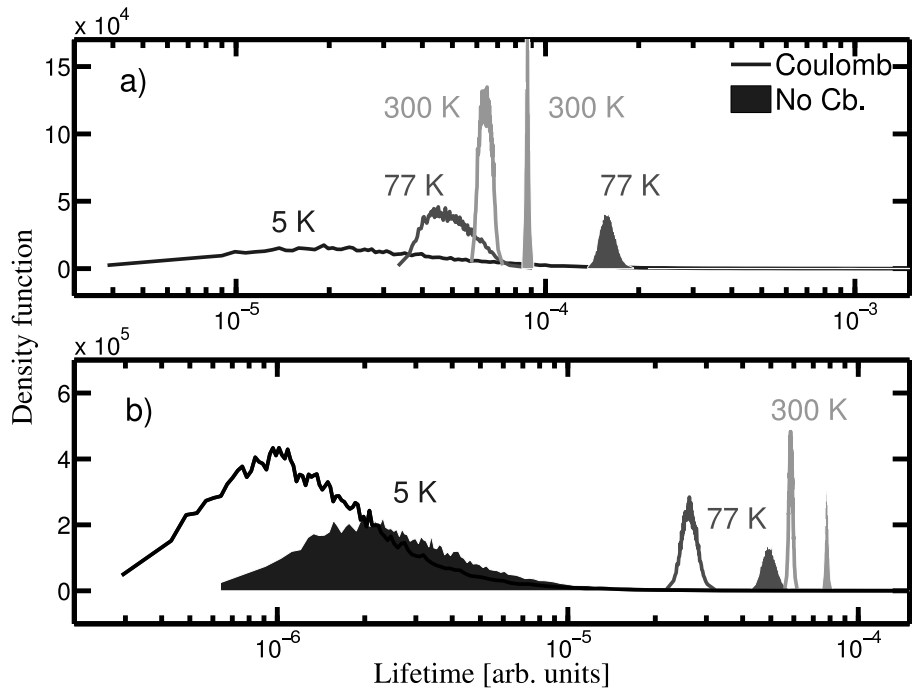


Fig. 13. Radiative lifetime distributions for an a) indirect-based model and b) the direct-based one for various temperatures in the case of weak disorder,  $W/J = 1$ .

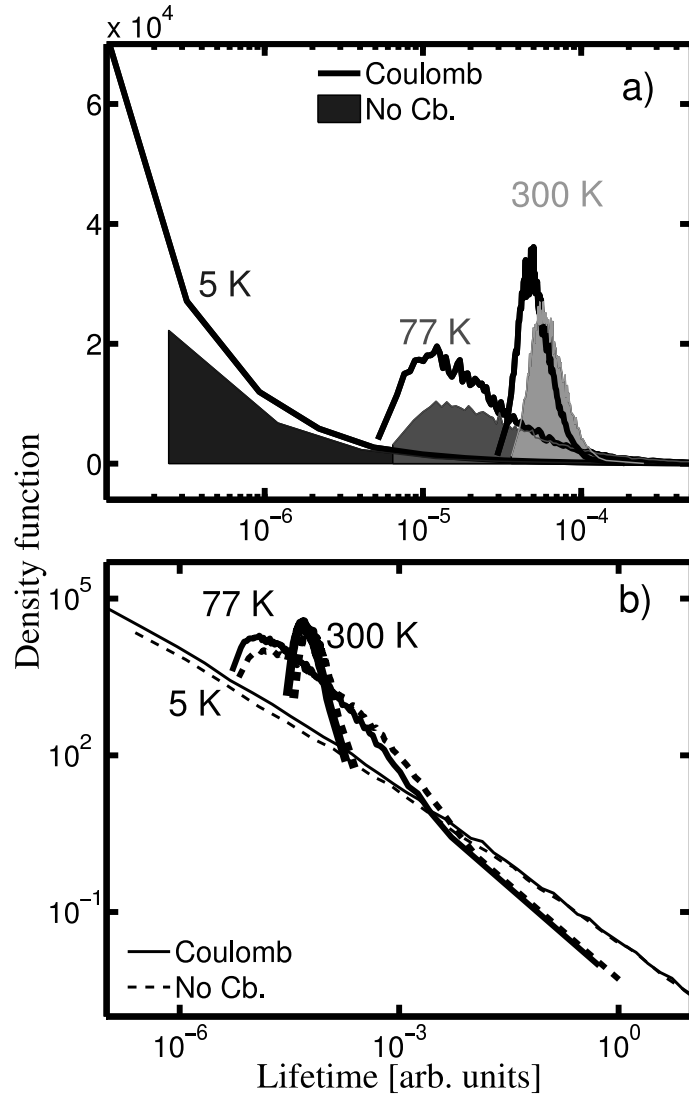


Fig. 14. Radiative lifetime distributions for an indirect-based model and for various temperatures for strong disorder,  $W/J = 16$ , on a) semilog and b) double-logarithmical plots.